Low-temperature Synthesis, Structural Characterization, and Electrochemistry of Ni-rich Spinel-like $LiNi_{2-y}Mn_yO_4$ ($0.4 \le y \le 1$)

Wang Hay Kan[1], Ashfia Huq[2], and Arumugam Manthiram[1,*]

[1]Materials Science and Engineering Program & Texas Materials Institute, The University of Texas at Austin, Austin, TX, USA

[2]Neutron Scattering Science Division, Oak Ridge National Laboratory, Oak Ridge, TN, USA

ABSTRACT: The thermal conversion of chemically delithiated layered $Li_{0.5}Ni_{1-y}Mn_yO_2$ ($0.2 \le y \le 0.5$) into spinel-like $LiNi_{2-y}Mn_yO_4$ ($0.4 \le y \le 1$) has been systematically investigated. The formed spinel-like phases are metastable and cannot be accessed by conventional high-temperature solid-state method. The layered to spinel transformation mechanism has been studied by the Rietveld refinement of *in-situ* neutron diffraction as a function of temperature (25 to 300 °C). In particular, the ionic diffusion of Li and M ions is quantified at different temperatures. Electrochemistry of the metastable spinel-like phases obtained has been studied in lithium-ion cells. Bond valence sum map has been performed to understand the ionic diffusion of lithium ions in the Ni-rich layered, spinel, and rock-salt structures. The study can aid the understanding of the possible phases that could be formed during the cycling of Ni-rich layered oxide cathodes.

1. INTRODUCTION

The current lithium-ion battery technology powers a wide range of modern devices (*e.g.,* cell phones and laptops) and electric vehicles.[1-5] The state-of-the art cathodes include layered $LiMO_2$ (M = transition metal), spinel $LiMn_2O_4$, and olivine $LiMPO_4$.[1-7] In particular, the spinel oxide is of great interest as the structure offers a 3D diffusion pathway for Li^+ ions and its small volume change during cycling.[8-10] Over the last two decades, however, the development of solid solutions with the normal spinel structure $Li_{(tect.,8a)}M_{2(oct.,16d)}O_{4(tect.,32e)}$ has been slow. For example, only $LiMn_{2-y}Co_yO_4$ ($0 \le y \le 1$) and $LiMn_{2-y}Ni_yO_4$ ($0 \le y \le 0.5$) have been reported for their structural analysis and electrochemistry in the Li-Mn-Ni-O and Li-Mn-Co-O systems.[11-17] A major reason is that LiM_2O_4 (M = Ni, Mn, Co, and their solid solutions) phases with Ni oxidation state > 2+ and Co oxidation state > 3+ are difficult to stabilize by the conventional high-temperature synthesis processes. In contrast, layered $LiMO_2$ (M = Ni, Mn, Co, and their solid solutions) phases with Ni oxidation state ≥ 2+ are relatively easier to stabilize by high-temperature processes (*e.g.,* $LiNi_{0.85}Co_{0.15}O_2$). Nonetheless, some layered compounds, *e.g.*, $LiMn_{1-x}Co_xO_2$, are yet to be reported, and Koyama's first principle study provided some insight on the insolubility issue.[12]

The spinel and layered structures are rather similar in which they both have the cubic close packed lattice of oxide ions (Fig. 1).[18,19] In the spinel phase, half of the octahedral sites are occupied by the transition-metal ions $M^{3.5+}$, and one eighth of the tetrahedral sites are occupied by lithium ions Li^+. While in the layered phase, half of the octahedral sites (*3b*) are occupied by transition-metal ions M^{3+}, and the other half (*3a*) are occupied by lithium ions in an ordered manner. In fact, the partially delithiated layered $Li_{0.5}MO_2$ phase is feasible to convert into the spinel LiM_2O_4 phase when one fourth of the transition-metal ions migrate from the octahedral site (*3b*) through the empty tetrahedral sites into the octahedral sites (*3a*) in the lithium layer, as show in Fig. 2. One of the most-known examples is the conversion of the layered $LiMnO_2$ into spinel $LiMn_2O_4$ upon cycling at room temperature; such a layered $LiMnO_2$ can be prepared by ionic exchange of α-$NaMnO_2$ with LiCl/LiBr.[20,21]

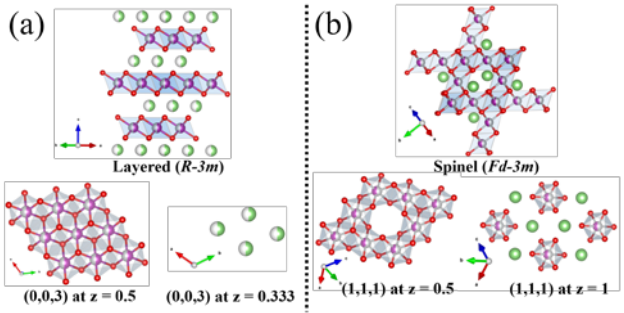

Fig. 1. Comparison the structural properties of layered (*R-3m*) and spinel (*Fd-3m*) phases.

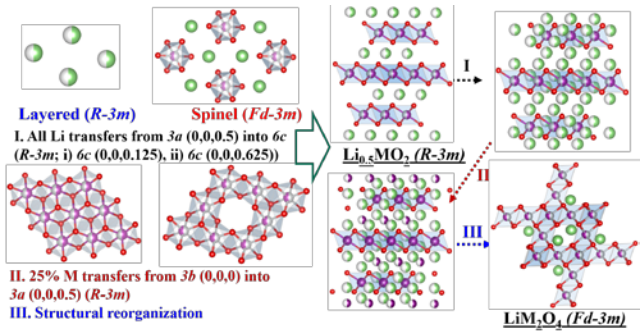

Fig. 2. Schematic diagrams showing how a layered compound can be transformed into a spinel phase, by promoting ionic diffusion (I and II) and structural reorganization (III).

In an attempt to enlarge the normal spinel phase diagram for the Li-Ni-Mn-O system, our strategy here is to obtain new meta-stable spinel phases by promoting the ionic diffusion of Li and M in the layered structure at intermediate temperatures (25-300 °C; Fig.2). For the first time, the layered to spinel transformation mechanism is captured by *in-situ* neutron diffraction of $Li_{0.5}Ni_{1-y}Mn_yO_2$ ($0.2 \le y \le 0.5$) between 25 and 300 °C. At much higher temperatures (>200 °C), the spinel phases are found to convert into rock-salt phases, which are not electrochemically active.

2. EXPERIMENTAL SECTION

2.1 Synthesis. $LiNi_{1-y}Mn_yO_2$ ($0.2 \le y \le 0.5$) samples were prepared by a sol-gel method. Stoichiometric amount of $Li(OAc)\cdot 2H_2O$, $Ni(OAc)_2\cdot 4H_2O$, $Mn(OAc)_2\cdot 4H_2O$ were first dissolved in distilled water and then maintained at 90 °C to form a sol/gel. The dried mixtures were decomposed at 450 °C, hand-grounded, and then further heat treated at 800 °C for 12 h in air. To prepare $Li_{0.5}Ni_{1-y}Mn_yO_2$ ($0.2 \le y \le 0.5$), the layered compounds were reacted with NO_2BF_4 in acetonitrile medium under Ar atm. for 12 h. The lithium content was confirmed by Inductively Coupled Plasma Atomic Emission Spectroscopy (ICP-AES).

2.2 Phase characterization. Phases were identified by powder X-ray diffraction (PXRD, Rigaku Ultima IV powder x-ray diffractometer, Cu K_α radiation, 40 kV, 44 mA) at 2θ = 10° to 80° at a count rate of 10 s per step of 0.02° at room temperature. Synchrotron X-ray diffraction was performed at ambient temperature at 2θ = 0.5° to 50° with a 2θ step size of 0.0001° with a monochromatic X-ray (λ = 0.414 Å) at the Advanced Photon Source (APS). The samples were packed into Kapton® Capillary Tube. *In-situ* time-of-flight neutron diffraction (ND) data were collected at the Oak Ridge National Laboratory (ORNL) Spallation Neutron Source (SNS) POWGEN beamline using a beam of neutron with a center wavelength of 1.333 Å (covering a d-spacing range of 0.4 to 5.4 Å). The samples were packed into a vanadium tube and the data were collected between 25 and 350 °C in a vacuum cryofurnace. The room temperature synchrotron X-ray and neutron datasets were refined by the conventional Rietveld method using the General Structure Analysis System (GSAS) package with the graphical user interface (EXPGUI).[22] The background, scale factor, zero (for X-ray only), absorption (for neutron only), cell parameters, atomic positions, thermal parameters and profile coefficients for Pseudo-Voigt / Finger, Cox, and Jephcoat (FCJ) Asymmetric peak shape function were refined until the convergence was achieved. Bond lengths were obtained by Bond Distance and Angle Computation (DISAGL) Version Win32 Crystal Structure Distance and Angle Program in the GSAS. The bond valences were calculated by Bond Valence Calculation and Listing (VaList).[23] The bond valence sum map was calculated by 3DBVSMAPPER.[24] Mass change/oxide-ion vacancy was analyzed in air with a NETZSCH Jupiter STA 449 F3 thermogravimetric analyzer.

2.3 Electrochemical performance. The active material (80 wt. %), super P (10 wt. %) and polyvinylidene fluoride (PVDF; 10 wt. %) were mixed in N-methyl-2-pyrrolidone (NMP) overnight and then coated onto an aluminium current collector. CR2032-type coin cells were then fabricated in an Ar-filled glove box with the cathode thus prepared, 1 M $LiPF_6$ in ethylene carbonate (EC)/diethyl carbonate (DEC) (1:1 by volume) as the electrolyte, and metallic lithium as the anode. The cells were cycled galvanostatically with an Arbin cycler from 4.9 to 2 V at a rate of 5 mAg^{-1}.

3. RESULTS AND DISCUSSION

3.1 Structural analysis of Ni-rich spinels. All the as-prepared layered $LiNi_{1-y}Mn_yO_2$ ($0.2 \le y \le 0.5$) compounds were found to be phase-pure and could be refined with a hexagonal *R-3m* space group by Rietveld refinement on synchrotron X-ray diffraction data (Fig. S1). From the joint X-ray and neutron Rietveld refinements on partially delithiated samples, approximately 4 to 8% of anti-site defect (*i.e.*, Li^+ in M site and vice versa) was found in the investigated samples. To understand the transformation from layered into spinel, the layered $LiNi_{1-y}Mn_yO_2$ samples were first partially delithiated with NO_2BF_4 in acetonitrile medium, and the Li content in the samples was confirmed by ICP-AES. Rietveld refinement of joint X-ray and neutron diffraction confirmed that all the partially delithiated $Li_{0.5}Ni_{1-y}Mn_yO_2$ ($0.2 \le y \le 0.5$) samples maintain the layered structure (Fig. 3.). The samples were subsequently analyzed by *in-situ* neutron diffraction between 25 and 350 °C.

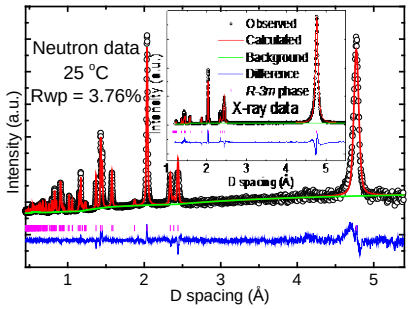

Fig. 3. Rietveld refinement of the joint X-ray and neutron diffractions of the partially delithiated $Li_{0.5}Ni_{0.8}Mn_{0.2}O_2$ at 25 °C.

As discussed above, a transformation of the layered structure into spinel structure requires ionic diffusions of Li^+ and $M^{3.5+}$ ions. To study such diffusion mechanism, a constraint was created in the Rietveld refinement in which Li^+ ions were allowed to occupy the octahedral (*3b*) and tetrahedral (*6c*) sites. Since the multiplicity of the octahedral site is half of that of the tetrahedral site, another constraint was made to reflect the increment of Li^+ ions in the *6c* sites, offsetting by twice the amount in the *3b* sites. In addition, all of the ions (Li/Ni/Mn/Co), located in the same crystallographic sites, were constrained to have the same thermal factors. Also, no significant amount of oxide-ion vacancies ($2O^{2-}_{(s)} \rightarrow O_{2(g)} + 4e^-$) was formed, as indicated by the negligible weight loss in the thermogravimetric analysis (TGA) plot (Fig. 4). Evaporation of lithium ion was unlikely to happen below 600 °C. Therefore, the total amounts of lithium and oxide ions in the samples were considered to be constant. Hereafter, the structural parameters (cell constant, atomic position, and thermal factor) were allowed to move freely until convergence was reached.

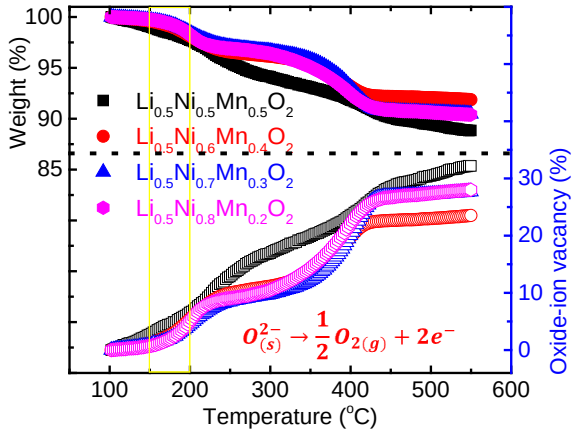

Fig. 4. Thermogravimetric analysis of $Li_{0.5}Ni_{1-y}Mn_yO_2$ ($0.2 \le y \le 0.5$) as a function of temperature. The corresponding oxide-ion vacancy in the samples was also calculated.

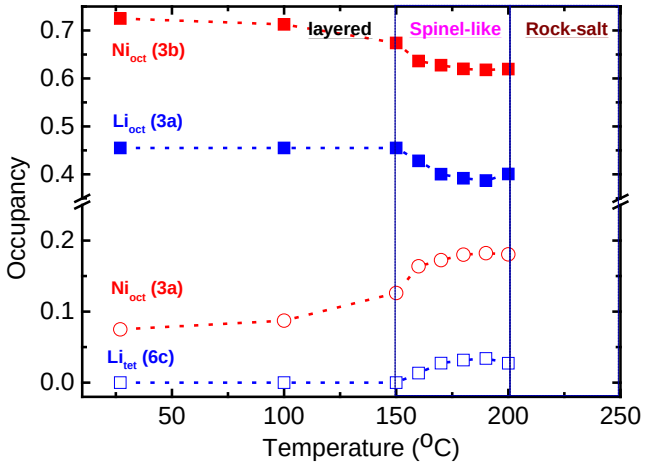

Fig. 5. Change in the occupancy of Ni and Li ions at (3a, 3b) and (3a and 6c), respectively, in $Li_{0.5}Ni_{0.8}Mn_{0.2}O2$ as a function of temperature.

An observable ionic diffusion was found at 100 °C or higher temperatures. Particularly, a movement of Ni ions from *3a* into *3b* sites and a displacement of Li ions from *3a* into *6c* sites were revealed (Fig. 5). Both increased steadily with temperature until about 190 °C. Reflecting to the diffraction patterns, the diffraction peaks (018) and (-120) of the layered structure, with the d spacing of ca. 1.4 to 1.5 Å, progressively merged into a single peak (022) of the spinel phase (Fig. S2). At 200 oC, the spinel-like phase had ca. 20% of the anti-site defect (Table 1, Tables S1 and S2). Such a spinel-like phase was found to be metastable, and was converted into a rock-salt phase at higher temperatures. Above 200 °C, the diffraction patterns could only be well fitted with a spinel (minor) and a rock-salt (major) phases (Fig. 6, Fig. S3 and S4). The results indicated that it was difficult to obtain high amounts of the spinel-like phase as the samples always contained various amount of layered and/or rock-salt phases.

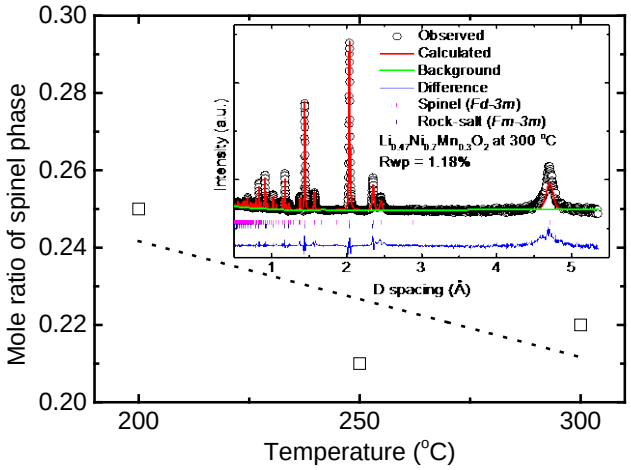

Fig. 6. Fractions of spinel and rock-salt phases in $Li_{0.53}Ni_{0.8}Mn_{0.2}O_2$ after heat-treating between 200 and 300 °C. The Rietveld refinement of $Li_{0.53}Ni_{0.8}Mn_{0.2}O_2$ after heat treating at 200 °C is shown in the inlet.

Table 1. Structural solution of Ni-rich spinel $LiNi_{1.6}Mn_{0.4}O_4$ prepared from $Li_{0.5}Ni_{0.8}Mn_{0.2}O_2$ at 200 °C for 12 h.

Atom	Fractional coordination	Occupancy	Multiplicity
Li	0.375, 0375, 0375	0.804(4)	8
Ni	0.375, 0375, 0375	0.196(4)	
Li	0, 0, 0	0.098(2)	
Mn	0, 0, 0	0.2	16
Ni	0, 0, 0	0.702(2)	
O	0.2375(5), 0.2375(5), 0.2375(5)	1	32

Layered $LiMnO_2$ is well-known to convert into spinel $LiMn_2O_4$ upon cycling. This motivated us to further study the role of Mn in the samples with different Mn content. Surprisingly, the ionic diffusion was found to decrease as

the Mn/Ni ratio increases (Fig. S5 and S6). Above 200 °C, the amount of rock-salt phase was found to increase with increasing Mn content. TGA analysis showed that the $Li_{0.5}Ni_{0.5}Mn_{0.5}O_2$ sample had significantly more oxide-ion vacancy (*i.e.*, weight loss) between 150 and 200 °C, a trigger for the formation of rock-salt phase.

Based on Deb's *in-situ* XANES analysis of $LiNi_{0.5}Mn_{0.5}O_2$, all Mn ions were found to be 4+ while Ni^{2+} ions were oxidized upon charging.[25] This made us assume that all Mn ions had a valence state of 4+ in the investigated samples $Li_{0.5}Ni_{1-y}Mn_yO_2$. Based on the stoichiometry, the oxidation states of Ni ions are, respectively, 3+ and 3.34+ in $Li_{0.5}Ni_{0.5}Mn_{0.5}O_2$ and $Li_{0.5}Ni_{0.8}Mn_{0.2}O_2$. The lower valent Ni ions favor their ions migration through the tetrahedral sites (Table S3),[18,19] due to the moderate octahedral-site-stabilization energy (OSSE) However, the tendency of Ni^{4+} ions to get reduced at elevated temperatures destabilizes the spinel stoichiometry and favors rock salt phase formation.

3.2 Electrochemical properties. The electrochemistry of the heat-treated samples $Li_{0.5}Ni_{1-y}Mn_yO_2$ ($0.2 \le y \le 0.5$; 150-200 °C) was analyzed with a coin-cell configuration. The cells were allowed to cycle between 2 and 4.9 V under a small current density of 5 mAh/g (Fig. 7). Interestingly, a sloping curve was observed for $Li_{0.5}Ni_{0.8}Mn_{0.2}O_2$ (150 °C) with a specific capacity of 110 mAh/g, a typical feature for layered cathodes. Upon further discharge, a new plateau was observed at ca. 2 V with a capacity of ca. 50 mAh/g. The second plateau was similar to the two-phase lithium ion insertion reaction in $Li_{1+z}NiO_2$ ($0 \le z \le 0.7$).[26] At 160 °C, the voltage for the sloping curve regions decreased slightly, but the voltage for the 2V plateau remained unchanged. The specific capacities were found to decrease to different extends.

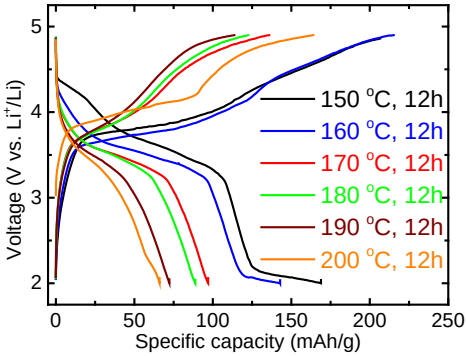

Fig. 7. Charge and discharge curves of the 2rd cycle of $Li_{0.5}Ni_{0.8}Mn_{0.2}O_2$ after heat-treating at 150 to 200 °C for 12 h.

For samples with higher Mn contents, the 2 V plateau was not observed, while the two sloping curves were present for all the temperature range. Similar to the $Li_{0.5}Ni_{0.8}Mn_{0.2}O_2$ sample, the cell voltage and capacity were found to decrease with increasing temperature (Figs. S7 and S8).

3.3 Ionic conduction pathway analysis. Direct observation of lithium-ion pathway is only feasible if the Li ions are ordered in different state of charge/discharge in the structure.[27] Such a transport information can be confirmed experimentally by measuring the anisotropic conductivity of a single crystal along different crystallographic directions.[28] An alternative method, called maximum entropy method (MEM) on *in-situ* neutron diffraction patterns, has also been used to study electrode materials (*e.g.*, Li_xFePO_4). Here we use a simple method called the bond valence sum (BVS) map to provide useful information about the ionic pathway This method can shed light on understanding the transport behavior of different ionic species (*e.g.*, Li^+, Na^+, O^{2-}).[24,29-31] Excellent examples can be found for garnet-type $Li_5La_3M_2O_{12}$ (M = Nb, Ta) and olivine-type $LiFePO_4$.[27,32]

To understand the conduction pathway for Li ions in the Ni-rich layered, spinel, and rock-salt phases, 3D bond valence sum (BVS) maps were constructed by assuming that all Mn ions were 4+ in both the layered and spinel phases. Also, the valences of Ni and Mn were assumed to be 2+ in the rock-salt phases. The contour plots of low bv mismatch were constructed to reveal the Li-ion pathways in the investigated samples.

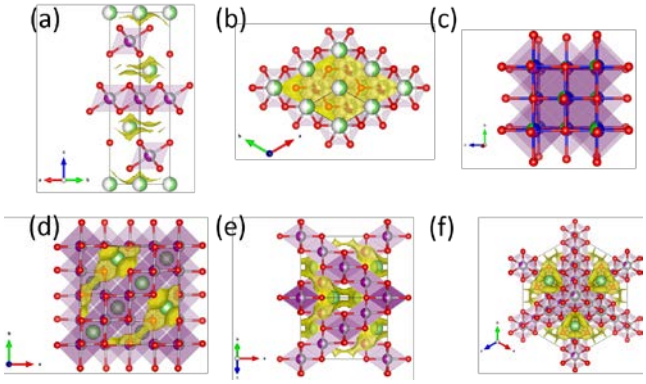

Fig. 8. 3D bond valence sum map of the Ni-rich layered oxide projected on (a) (110) and (b) (003) planes. The (100) plane in the rock-salt phase is shown in (c). The (100), (110), and (111) planes in the spinel phase are shown, respectively, in (d), (e), and (f).

As shown in Fig. 8, 2D, 3D and 0D pathways were revealed, respectively, for the Ni-rich layered $Li_{0.5}Ni_{0.5}Mn_{0.2}O_2$, spinel $LiNiMnO_4$, and rock-salt $Li_{0.33}Ni_{0.33}Mn_{0.33}O$ phases. The results are similar to the BVS maps of $LiCoO_2$ (*R-3m*), $LiMn_2O_4$ (*Fd-3m*) and NiO (*Fm-3m*). Although Ni-rich spinel with 3D Li ion conduction pathway is expected to have good electrochemical properties, our Rietveld refinement analysis clearly showed that the ionic diffusions were not fully completed to yield the non-defective spinels in all investigated samples. Such an imperfection created defects (*e.g.*, anti-site, vacancy) and the potential 3D ionic pathway was largely impeded.

Lastly, Mohanty *et al.* recently reported a similar phase transformation of layered-type $Li_{1.2}Mn_{0.55}Ni_{0.15}Co_{0.1}O_2$ into spinel phase, driven by cell

voltages and cyclings.[33] Zheng *et al.* observed such a phase transformation occurring on the surface by high resolution transmission electron microscopy (HR-TEM).[34] Although our study focused on the *in-situ* phase transformation at elevated temperatures, it is anticipated that Ni-rich layered compounds (*R-3m*) could undergo a similar degradation process through the formation of Ni-rich spinel and rock-salt phases, after long cycling at ambient condition.

In conclusion, this work provides an understanding on the possible phases that are formed on heating partially delithiated samples at moderate temperatures. The results could become useful on subjecting Ni-rich layered oxides to prolonged cycling, particularly at elevated temperatures.

ASSOCIATED CONTENT

Neutron diffraction pattern and PXRD analysis. Electrochemistry data.

AUTHOR INFORMATION

Corresponding Author

* E-mail: manth@austin.utexas.edu

Funding Sources

National Science Foundation Materials Interdisciplinary Research Team (MIRT) grant DMR-1122603.

Notes

The authors declare no competing financial interest.

ACKNOWLEDGMENT

National Science Foundation Materials Interdisciplinary Research Team (MIRT) grant DMR-1122603 and the Welch Foundation grant F-1254. The *in-situ* neutron diffraction measurement at the POWGEN beamline at the Oak Ridge National Laboratory's (ORNL) Spallation Neutron Source (SNS) was sponsored by the Scientific User Facilities Division, Office of Basic Energy Sciences, US Department of Energy. The authors appreciate the useful discussion with Drs. Melanie Kirkham and Pamela Whitfield at the POWGEN in ORNL, and Drs. Jianming Zheng and Bohang Song at the University of Texas at Austin. Use of the Advanced Photon Source at Argonne National Laboratory was supported by the U. S. Department of Energy, Office of Science, Office of Basic Energy Sciences, under Contract No. DE-AC02-06CH11357.

REFERENCES

(1) Goodenough, J. B.; Manthiram, A. A perspective on electrical energy storage. *MRS Commun.* **2014**, *4*, 135-142.
(2) Manthiram, A. Materials Challenges and Opportunities of Lithium Ion Batteries. *J. Phys. Chem. Lett.* **2011**, *2*, 176-184.
(3) Manthiram, A. In *Tilte*2004; Kluwer Academic Publishers.
(4) Manthiram, A.; Chemelewski, K.; Lee, E.-S. A perspective on the high-voltage LiMn1.5Ni0.5O4 spinel cathode for lithium-ion batteries. *Energy Environ. Sci.* **2014**, *7*, 1339-1350.
(5) Manthiram, A.; Muraliganth, T. In *Tilte*2011; Wiley-VCH Verlag GmbH & Co. KGaA.
(6) Padhi, A. K.; Nanjundaswamy, K. S.; Goodenough, J. B. Phospho-olivines as positive-electrode materials for rechargeable lithium batteries. *J. Electrochem. Soc.* **1997**, *144*, 1188-1194.
(7) Padhi, A. K.; Nanjundaswamy, K. S.; Masquelier, C.; Okada, S.; Goodenough, J. B. Effect of structure on the Fe3+/Fe2+ redox couple in iron phosphates. *J. Electrochem. Soc.* **1997**, *144*, 1609-1613.
(8) David, W. I. F.; Thackeray, M. M.; De Picciotto, L. A.; Goodenough, J. B. Structure refinement of the spinel-related phases lithium manganese oxides (Li2Mn2O4) and Lio.2Mn2O4). *J. Solid State Chem.* **1987**, *67*, 316-323.
(9) Thomas, M. G. S. R.; David, W. I. F.; Goodenough, J. B.; Groves, P. Synthesis and structural characterization of the normal spinel lithium nickel oxide (Li[Ni2]O4). *Mater. Res. Bull.* **1985**, *20*, 1137-1146.
(10) Xiong, L.; Xu, Y.; Tao, T.; Song, J.; Goodenough, J. B. Excellent stability of spinel LiMn2O4-based composites for lithium ion batteries. *J. Mater. Chem.* **2012**, *22*, 24563-24568.
(11) Kobayashi, H.; Sakaebe, H.; Kageyama, H.; Tatsumi, K.; Arachi, Y.; Kamiyama, T. Changes in the structure and physical properties of the solid solution LiNi1-xMnxO2 with variation in its composition. *J. Mater. Chem.* **2003**, *13*, 590-595.
(12) Koyama, Y.; Makimura, Y.; Tanaka, I.; Adachi, H.; Ohzuku, T. Systematic Research on Insertion Materials Based on Superlattice Models in a Phase Triangle of LiCoO2-LiNiO2-LiMnO2. *J. Electrochem. Soc.* **2004**, *151*, A1499-A1506.
(13) Nitta, Y.; Okamura, K.; Haraguchi, K.; Kobayashi, S.; Ohta, A. Crystal structure study of LiNi1-xMnxO2. *J. Power Sources* **1995**, *54*, 511-515.
(14) Kim, S.-K.; Yang, D.-H.; Sohn, J.-S.; Jung, Y.-C. Resynthesis of LiCo1-xMnxO2 as a cathode material for lithium secondary batteries. *Met. Mater. Int.* **2012**, *18*, 321-326.
(15) Suresh, P.; Rodrigues, S.; Shukla, A. K.; Vasan, H. N.; Munichandraiah, N. Synthesis of LiCo1-xMnxO2 from a low-temperature route and characterization as cathode materials in Li-ion cells. *Solid State Ionics* **2005**, *176*, 281-290.
(16) Waki, S.; Dokko, K.; Itoh, T.; Nishizawa, M.; Abe, T.; Uchida, I. High-speed voltammetry of Mn-doped LiCoO2 using a microelectrode technique. *J. Solid State Electrochem.* **2000**, *4*, 205-209.
(17) Yanase, I.; Ohtaki, T.; Watanabe, M. Application of combinatorial process to LiCo1-xMnxO2 ($0 \le x \le 0.2$) powder synthesis. *Solid State Ionics* **2002**, *151*, 189-196.
(18) Choi, S.; Manthiram, A. Factors influencing the layered to spinel-like phase transition in layered oxide cathodes. *J. Electrochem. Soc.* **2002**, *149*, A1157-A1163.
(19) Chebiam, R. V.; Prado, F.; Manthiram, A. Structural instability of delithiated Li1-xNi1-yCoyO2 cathodes. *J. Electrochem. Soc.* **2001**, *148*, A49-A53.
(20) Armstrong, A. R.; Bruce, P. G. Synthesis of layered LiMnO2 as an electrode for rechargeable lithium batteries. *Nature (London)* **1996**, *381*, 499-500.
(21) Vitins, G.; West, K. Lithium intercalation into layered LiMnO2. *J. Electrochem. Soc.* **1997**, *144*, 2587-2592.
(22) Toby, B. H. EXPGUI, a graphical user interface for GSAS. *J. Appl. Crystallogr.* **2001**, *34*, 210-213.
(23) Brown, I. D.; Shannon, R. D. Empirical bond-strength-bond-length curves for oxides. *Acta Crystallogr., Sect. A* **1973**, *29*, 266-282.

(24) Sale, M.; Avdeev, M. 3DBVSMAPPER: a program for automatically generating bond-valence sum landscapes. *J. Appl. Crystallogr.* **2012**, *45*, 1054-1056.
(25) Deb, A.; Bergmann, U.; Cramer, S. P.; Cairns, E. J. Local structure of LiNi0.5Mn0.5O2 cathode material probed by in situ x-ray absorption spectroscopy. *J. Appl. Phys.* **2006**, *99*, 063701/063701-063701/063710.
(26) Dahn, J. R.; Von Sacken, U.; Michal, C. A. Structure and electrochemistry of lithium nickel oxide (Li1±yNiO2 and a new Li2NiO2) phase with the nickel hydroxide (Ni(OH)2) structure. *Solid State Ionics* **1990**, *44*, 87-97.
(27) Nishimura, S.-i.; Kobayashi, G.; Ohoyama, K.; Kanno, R.; Yashima, M.; Yamada, A. Experimental visualization of lithium diffusion in LixFePO4. *Nat. Mater.* **2008**, *7*, 707-711.
(28) Li, J.; Yao, W.; Martin, S.; Vaknin, D. Lithium ion conductivity in single crystal LiFePO4. *Solid State Ionics* **2008**, *179*, 2016-2019.
(29) Bo, S.-H.; Grey, C. P.; Khalifah, P. G. Defect-Tolerant Diffusion Channels for Mg2+ Ions in Ribbon-Type Borates: Structural Insights into Potential Battery Cathodes MgVBO4 and MgxFe2-xB2O5. *Chem. Mater.* **2015**, *27*, 4630-4639.
(30) Fujii, K.; Esaki, Y.; Omoto, K.; Yashima, M.; Hoshikawa, A.; Ishigaki, T.; Hester, J. R. New Perovskite-Related Structure Family of Oxide-Ion Conducting Materials NdBaInO4. *Chem. Mater.* **2014**, *26*, 2488-2491.
(31) Kan, W. H.; Huq, A.; Manthiram, A. The first Fe-based Na+-ion cathode with two distinct types of polyanions: Fe3P5SiO19. *Chem. Commun. (Cambridge, U. K.)* **2015**, *51*, 10447-10450.
(32) Thangadurai, V.; Adams, S.; Weppner, W. Crystal Structure Revision and Identification of Li+-Ion Migration Pathways in the Garnet-like Li5La3M2O12 (M = Nb, Ta) Oxides. *Chem. Mater.* **2004**, *16*, 2998-3006.
(33) Mohanty, D.; Li, J.; Abraham, D. P.; Huq, A.; Payzant, E. A.; Wood, D. L.; Daniel, C. Unraveling the Voltage-Fade Mechanism in High-Energy-Density Lithium-Ion Batteries: Origin of the Tetrahedral Cations for Spinel Conversion. *Chem. Mater.* **2014**, *26*, 6272-6280.
(34) Zheng, J.; Xu, P.; Gu, M.; Xiao, J.; Browning, N. D.; Yan, P.; Wang, C.; Zhang, J.-G. Structural and Chemical Evolution of Li- and Mn-Rich Layered Cathode Material. *Chem. Mater.* **2015**, *27*, 1381-1390.

TABLE OF CONTENTS